

# 3D Simulation of resistance welding processes and weld strength testing

**Nielsen, Chris Valentin; Zhang, Wenqi**

*Published in:*
Simulationsforum 2013: Schweissen und Wärmebehandlung

*Publication date:*
2013

# 3D Simulation of Resistance Welding Processes and Weld Strength Testing

Chris V. Nielsen and Wenqi Zhang
SWANTEC Software and Engineering ApS
DK-2800 Kongens Lyngby
Denmark

**Abstract**

This paper summarizes the new developments in 3D simulation of resistance welding processes and the subsequent weld strength testing based on the predicted weld results and material properties after welding. Resistance welding simulations have been developed and applied for prediction of weld nugget formation in spot welding as well as projection welding with various material combinations. Microstructure and hardness distributions are also modeled for predicting the material properties in and around the weld zone after welding. Some examples are presented for industrial applications of 3D resistance welding simulations.

## 1. Introduction

Resistance welding is widely applied in a number of industries for effective and productive joining of metal components. Spot welding and a number of different types of projection welding are used in the assembly of automotives. The process is also widely applied in a number of other industries e.g. including electronic components.

The welding engineers in the different industries meet challenges related to new materials, changing geometries as well as demanding quality, cost and robustness. This requires large amounts of testing and validation of new weld schedules and eventual geometrical changes when it comes to projection welding. Numerical simulation is a tool that helps the engineers to understand complicated processes by visualization, and it is a tool for setting up and testing new designs and welding parameters. As an outcome, the amount of testing is reduced significantly and the time to market can be reduced.

Since the first version of SORPAS® in 1999, computer simulations have helped welding engineers setting up weldability lobes, selecting welding parameters and suggest alternative current and force profiles for welding specific material combinations including new materials such as advanced high strength steels (AHSS), ultra high strength steels (UHSS) and aluminium alloys [1-6]. Latest developments of SORPAS® include a fully automated function for suggesting welding parameters as a starting point for the welding engineers, while also estimating the window of acceptable weld currents as a measure of robustness. Simulation of adhesives and non-conducting layers are examples of other new developments to support the innovations in industry [7].

Spot welding and ring projections have for many years been analyzed and optimized using SORPAS® 2D, which is supplying axisymmetric simulations (or eventual block model simulations). New developments in the software and appearance of faster computers allow simulation of more complex geometries with the newly launched SORPAS® 3D [5-6]. In relation to spot welding, three dimensional analyses are relevant in the modeling of e.g. electrode misalignment, welding near previous spots and welding near edges. It is also possible to simulate weld strength testing in terms of the standard tensile-shear, cross-tension and peel testing, and it is possible to simulate the deformation behaviour and strength of multiple spots under certain loadings. Furthermore, SORPAS® 3D opens a new field of projection welding simulations that in many cases involve geometries with complexity in 3D.

The remaining paper presents briefly the governing equations of the basic models followed by numerous examples of 3D simulations of resistance welding including weld strength testing.

## 2. Coupled electro-thermo-mechanical finite element formulation

The core of the finite element program is a coupled electro-thermo-mechanical formulation [5]. The mechanical model is responsible for deformation and stress distribution, while the electrical model is responsible for the distribution of the current density giving rise to heat generation by Joule heating. The temperature distribution and changes in material properties due to temperature are solved in the thermal model.

The mechanical model is based on the irreducible flow formulation [8], which in weak form suited for finite element implementation can be stated as,

$$\delta\Pi = \int_V \overline{\sigma}\delta\dot{\overline{\varepsilon}}dV + K\int_V \dot{\varepsilon}_V\delta\dot{\varepsilon}_V dV - \int_S t_i\delta u_i dS + \sum_{c=1}^{N_c} Pg_c\delta g_c \tag{1}$$

where $\delta$ indicates an arbitrary admissible variation in the velocity field, $\Pi$ is the energy rate of the system, $V$ is the domain volume with surface $S$, $\overline{\sigma}$ is the effective stress and $\dot{\overline{\varepsilon}}$ is the equivalent strain rate. The second term is to obey volume constancy in the plastic formulation by penalizing the volumetric strain rate $\dot{\varepsilon}_V$ by a large positive constant $K$. The third term is eventual surface tractions $t_i$ on surface with velocity $u_i$. Finally, the fourth term is to obey mechanical contact between objects (workpieces, electrodes etc.) by penalizing normal velocity difference $g_c$ in contact pair $c$ (if otherwise resulting in penetration) by a large positive constant $P$. A contact pair consists of a node from one side of the contact and an element face of the other side (see details of the contact implementation elsewhere [5,9]).

The thermal model responsible for the temperature field $T$ is governed by

$$kT_{,ii} + \dot{q} = \rho c\dot{T} \tag{2}$$

with thermal conductivity $k$, mass density $\rho$ and heat capacity $c$. The heat generation is included by $\dot{q}$, which is the link to the electrical model generating heat according to Joule heating based on the electrical resistance and the current density (squared). The current density field is available from the gradient of the potential $\Phi$ solved in the electrical model by

$$\Phi_{,ii} = 0 \tag{3}$$

which in its form is identical to the stationary part of (2) because the transient part of the electrical field can be ignored compared to the transient response of the temperature field.

Contact resistance, being critical for the modeling of resistance welding, is evaluated based on the strength of the materials at the given temperature, the contact pressure and the electrical properties including restriction of the current and surface contamination in form of oxides, oils, films etc. [2-3].

## 3. Weld properties and weld strength testing

While completing the welding simulation including cooling, the history of temperature at all nodal points are obtained and the cooling rates can be calculated. According to the continuous cooling transformation (CCT) diagrams, the microstructures can be modelled to obtain the distributions of martensite, bainite, pearlite and ferrite. The phases present in the weld nugget are based on weighted volume mixing of the

materials melted in the nugget, assuming full mixing inside the nugget. The hardness distribution is obtained by the contributions of the predicted phases by applying the model by Blondeau et al. [10], knowing the actual cooling rates and the carbon equivalent. Further details on microstructure and hardness evaluation including comparison with experiments can be found in reference [11].

Figure 1a shows an example of the temperature history in two selected nodes. Cooling rates at any time and temperature are available for each node. Figure 1b shows an example of simulated hardness. The simulation of hardness distribution is able to capture both hardening and softening in the heat affected zone.

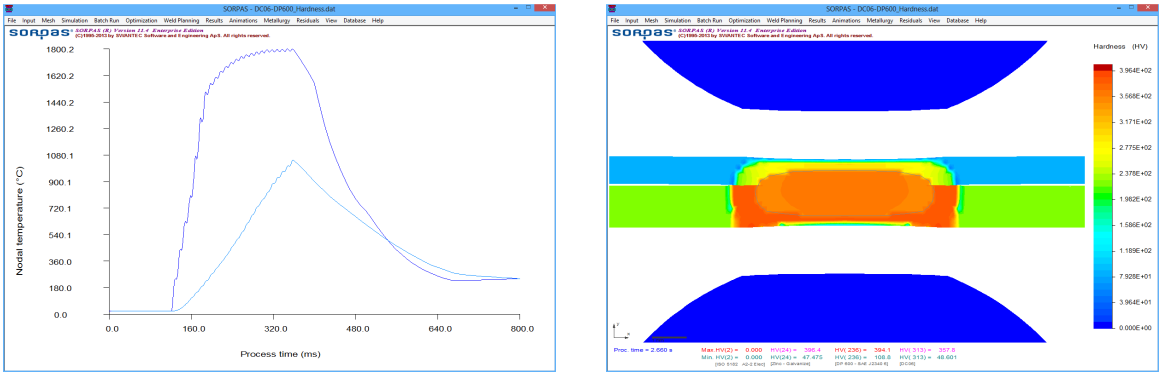


(a) (b)

*Figure 1: Simulation of microstructures and hardness distribution in spot welding of DC06 to DP600. (a) Temperature history at two nodal points, by which the cooling rates can be obtained. (b) Simulated hardness distribution.*

With the recent developments in 3D simulation of resistance welding, it is now possible to expand the numerical analysis of spot welding to include subsequent mechanical testing. The mechanical testing includes the standard mechanical tests: tensile-shear, cross-tension and peel testing (see Figures 2a, 2b and 2c, respectively), but can also be used to analyze any other complicated loading situation or the strength of a combination of multiple spots.

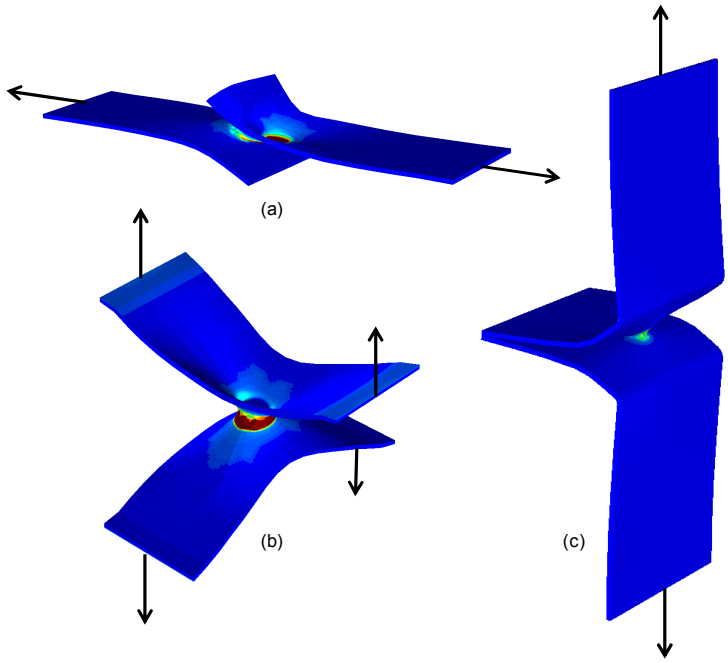


*Figure 2: Examples of simulated tensile testing by (a) tensile-shear test, (b) cross-tension test and (c) peel test.*

Combining the simulation of welding and testing makes it possible to simulate the testing based on the predicted nugget size and shape, the predicted microstructure and hardness distribution. In SORPAS® 3D the combined simulation is prepared through an integrated wizard and the simulation is carried out without intermediate stop as the electrodes are automatically removed and the tool connections are changed from the welding machine to the testing machine according to the selection before the simulation is started. This is a new strategy introduced in SORPAS® 3D as opposed to other simulations of weld strength, where either a rigid weld nugget is assumed or an assumed stress field is imposed.

Figures 3 and 4 include examples of simulated welds followed by tensile-shear testing. Two DC06 sheets of 0.8mm (Figure 3) and two DC06 sheets of 3.0mm (Figure 4) are analyzed. The simulated weld nuggets are shown in the upper part of the figures followed by the load-elongation curves including the evolution of deformation and damage at selected points on the curve. Finally the lower parts of the figures show the final deformation of ended testing including the distribution of damage.

Such simulations allow prediction of failure mode and strength. The thin sheets has a resulting plug failure, where the damage, thinning of the sheet and finally fracture (dark red area) take place outside the nugget leaving an undamaged button shaped piece of sheet on one side. On the other hand, the resulting failure mode between the thick sheets is an interface failure, where the sheets bend, but with minimal damage, while damage develops in the nugget between the sheets, and finally the joint breaks at the interface.

The maximum load and corresponding elongation are available from the curves as well (notice the different scales on the two curves when comparing Figures 3 and 4).

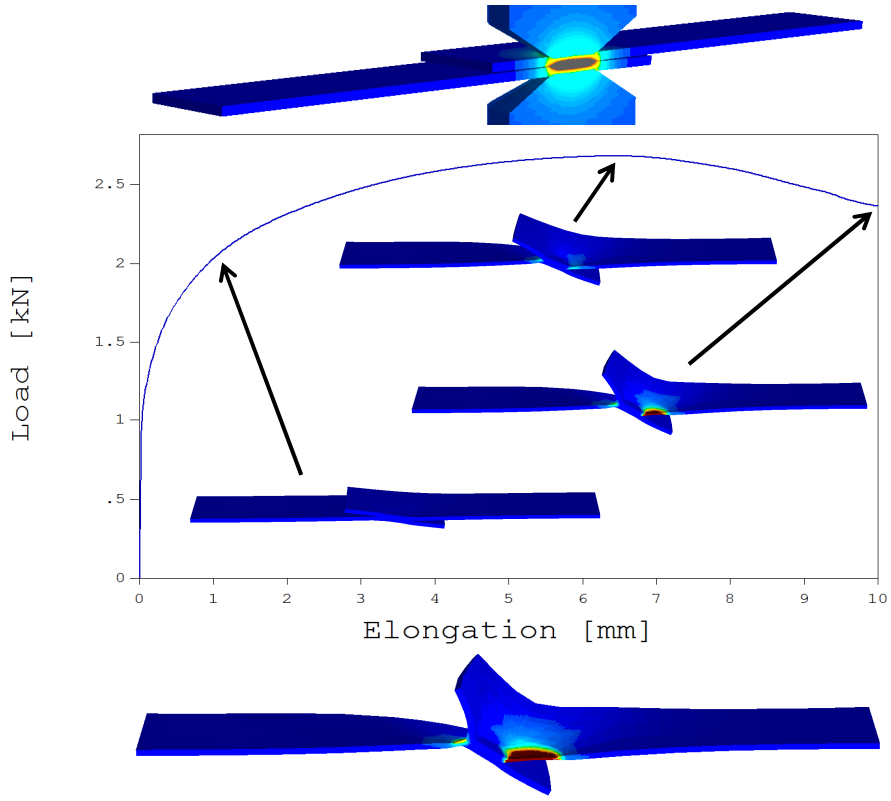


*Figure 3: Spot welding of 0.8mm DC06-DC06 followed by tensile shear testing.*

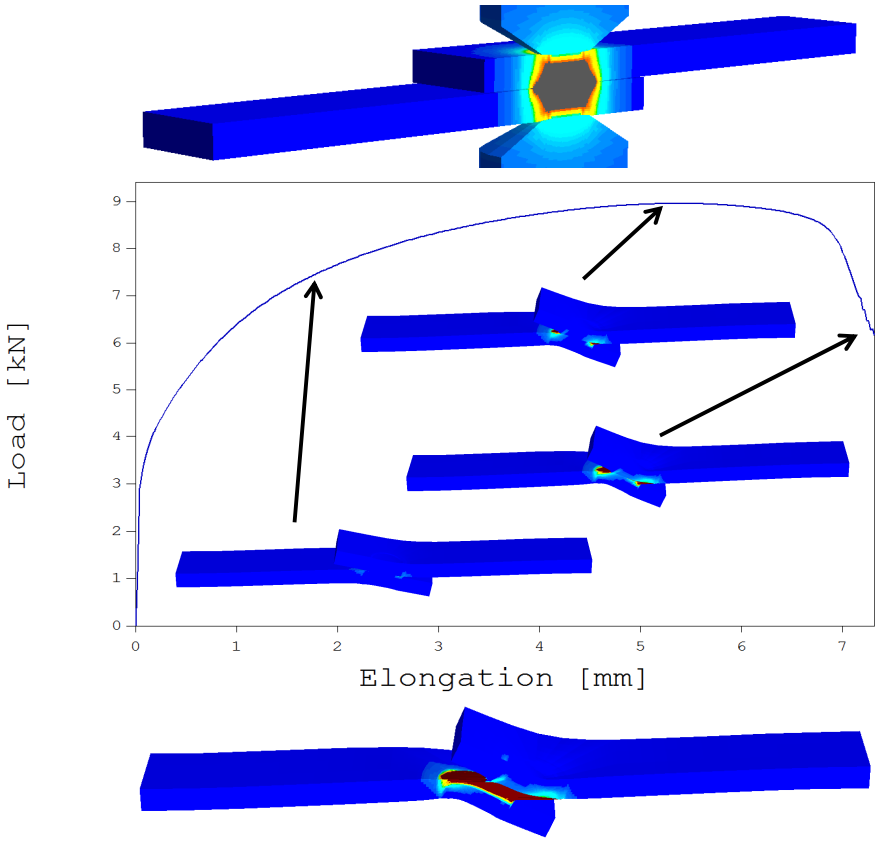


*Figure 4: Spot welding of 3.0mm DC06-DC06 followed by tensile shear testing.*

## 4. Evaluation of shunt effects

Besides the above weld strength testing, 3D simulation also expands the possibilities of analysis of the welding process itself. In terms of spot welding, effects such as electrode misalignment, shunt effects and single sided spot welding of sheets to tubular structures require 3D analysis for complete modeling [5,12]. Among these, shunt effects between three spots are shown as an example in the following.

Figure 5 shows the temperature fields after the end of the weld time at the three different locations. The first weld has the full current passing through the weld spot forming a nugget with diameter 5.75mm. When welding the second spot, part of the current will pass through the first spot due to the formed connection. As a result of this shunt effect, the effective welding current is lowered and the second nugget diameter is reduced to 5.31mm. The third nugget diameter reaches only 5.04mm due to shunting through both of the previously welded spots. The differences in nugget sizes are visible in the lower part of Figure 5, where the overall process peak temperature is shown together with the final weld nuggets.

The amount of current passing through previous spots and the effective current passing through the spot being welded are presented in Figure 6, where also the current density at an instant of time during the third weld in shown. The current distribution shows how current passes through the sheets to go through previous spots and forming high current density along the ring of the edge of the spots.

From the curves in Figure 6 it can be stated how much of the total current that passes through each individual weld point. During the time of the first weld, it is confirmed that 100% of the current passes through the first point while no current passes through the other weld locations as the sheets are still separated at this time. Then, in rough numbers, 90% of the weld current passes through the second spot

during the time of the second weld, while the remaining 10% goes through the first spot, which is now acting as a connection point. Finally during the third weld, and still in rough numbers, only 80% of the total current flows through the third point, while the remaining current is distributed over the previous two spots.

The simulation would also allow the selection of individual weld programs for each weld. In this case, proper selection (increase) of the weld current can result in identical weld nugget sizes.

The shunt current passing through previous spots also has a heating effect. Figure 7 shows this by a nodal temperature curve showing the temperature as function of time for a selected location at the edge of the first spot. During the time of the first weld, the temperature is of course increasing, reaching a maximum before it starts cooling. Then, during the second and third welds, current passes through the point due to shunting and the temperature is shortly raised again.

It can be of interest to know the level of the temperature reached in previous spots. Depending on the time and distance between spots, the temperature may affect the formation of the microstructure and final hardness of the welds and heat affected zones.

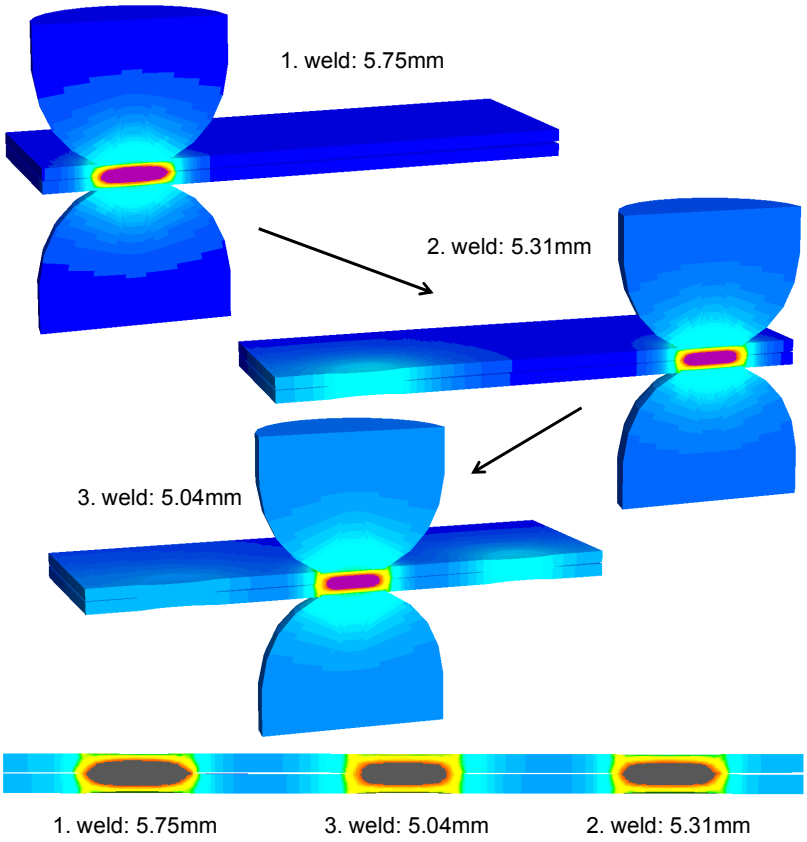


*Figure 5: Temperature fields at the end of the weld time for three spot welds near each other. With identical total current input, the first weld reaches 5.75mm nugget diameter, while the second and third only reaches 5.31mm and 5.04mm due to shunt effects. The lower figure shows the overall process peak temperature and the resulting weld nuggets.*

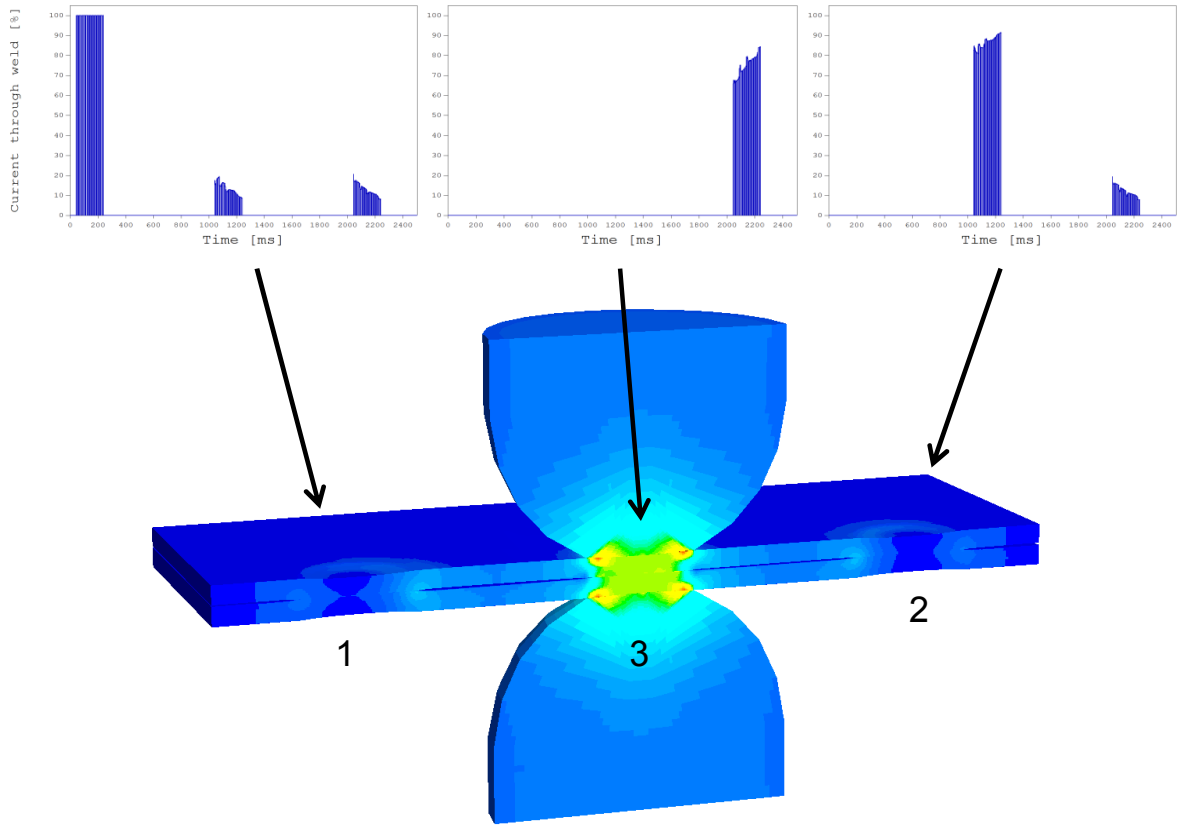


*Figure 6: Curves of percentage of total current passing through the interface at each of the three weld locations. The lower figure shows the current distribution at an instant of time during the third spot weld. The shunt effect is visualized by the current passing through the two previously welded spots.*

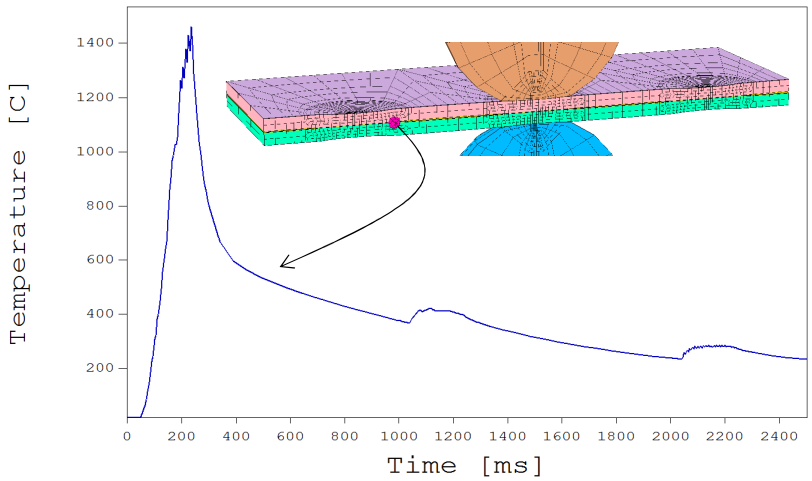


*Figure 7: Nodal temperature of selected point at the edge of the first weld.*

## 5. Projection welding

A large part of projection welding cases is naturally simulated in 3D because of the geometrical complexity. Two examples are provided in Figure 8 for illustration by the initial geometry and the final deformation and peak temperature field. Figure 8a includes a square nut welded to a sheet, and Figure 8b is an example of two sheets welded perpendicular to each other by means of a longitudinal embossment pressed in one of the sheets. Such simulations are typically more demanding in terms of mechanical modeling due to the large deformations involved compared to spot welding.

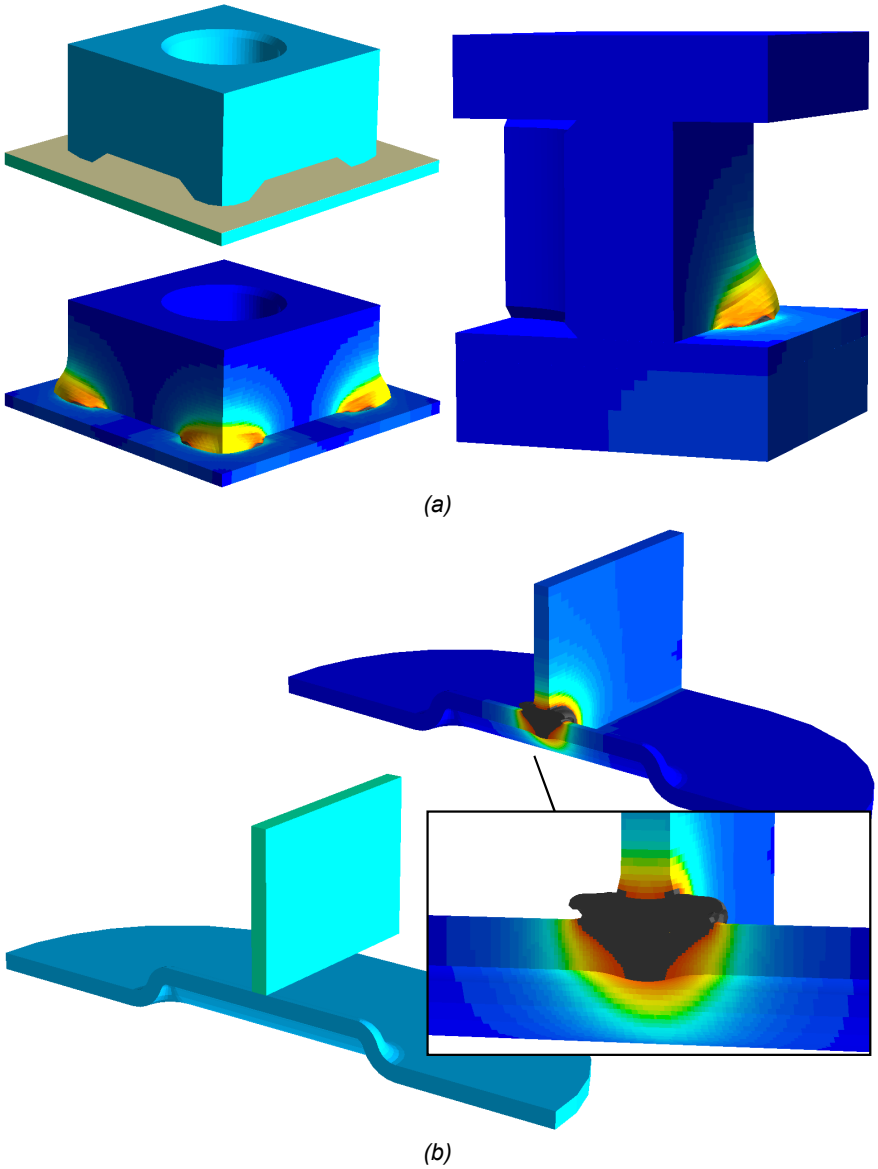

*Figure 8: Examples of simulated projection welds by (a) square nut welded to sheet and (b) sheet welded perpendicular to a sheet with a longitudinal embossment.*

## 6. Conclusions

An overview of typical cases analyzed by 3D finite element simulations is provided in the paper drawing from spot welding and weld strength testing to projection welding. The cases were selected to illustrate some of the potential analyses that can be conducted by simulation in 3D. Adding the third dimension, compared to more classical 2D simulations, expands the possibilities in terms of cases that can be simulated, details that can be examined, and also continuation by weld strength testing. It is, however, important to keep in mind when 3D simulations should be utilized and when 2D simulations are more attractive due to computation speed and easy setup of geometries. Although, parallel computing with multiple processors has been implemented for 3D simulation to speed up the calculations, the computation time is still much longer than that of 2D. Therefore, the 3D simulations are useful mainly for complex welding cases, while the 2D simulations are more suitable for optimizations of spot welding and simple projection welding applications.

## References


[1] W. Zhang, H. Hallberg and N. Bay. Finite Element Modeling of Spot Welding Similar and Dissimilar Metals. 7th Int. Conf. on Computer Technology in Welding, San Francisco, USA, p.364-373, 1997.

[2] W. Zhang and L. Kristensen. Finite Element Modeling of Resistance Spot and Projection Welding Processes. The 9th Int. Conf. on Computer Technology in Welding, Detroit, Michigan, p.15-23, 1999.

[3] W. Zhang. Design and Implementation of Software for Resistance Welding Process Simulations. SAE 2003 Transactions: Journal of Materials and Manufacturing, Vol.112, No.5, 2003, p.556-564, 2003.

[4] C. V. Nielsen, K. S. Friis, W. Zhang, and N. Bay. Three-Sheet Spot Welding of Advanced High-Strength Steels. Welding Journal Research Supplement, Vol. 90 No. 2, p.32s-40s, 2011.

[5] C.V. Nielsen, W. Zhang, L.M. Alves, N . Bay and P.A.F. Martins: Modeling of Thermo-Electro-Mechanical Manufacturing Processes with Applications in Metal Forming and Resistance Welding. Published by Springer, 2013.

[6] Information on http://www.swantec.com.

[7] W. Zhang, A. Chergui and C.V. Nielsen. Process Simulation of Resistance Weld Bonding and Automotive Light-weight Materials. Proceedings of the 7th International Seminar on Advances in Resistance Welding. Busan, Korea, p.67-75, 2012.

[8] M.L. Alves, J.M.C. Rodrigues, and P.A.F. Martins: Simulation of three-dimensional bulk forming processes by finite element flow formulation, Modelling and Simulation in Materials and Engineering – Institute of Physics 11, p.803-821, 2003.

[9] C.V. Nielsen, P.A.F. Martins, W. Zhang, and N. Bay: Mechanical contact experiments and simulations, Steel Research International 82, p.645-650, 2011.

[10] R. Blondeau, P. Maynier, J. Dollet. Prediction of the hardness and strength of plain and low-alloy steels from their structure and composition. Memoires Scientifiques de la Revue de Metallurgie, Vol. 70, No. 12, p.883-892, 1973.

[11] K.R. Pedersen, A. Harthoej, K.L. Friis, N. Bay, M.A.J. Somers and W. Zhang. Microstructure and hardness distribution of resistance welded advanced high strength steels. Proceedings of the 5th International Seminar on Advances in Resistance Welding. Toronto, Canada, p.134-146 2008

[12] C.V. Nielsen, A. Chergui and W. Zhang: Single-sided sheet-to-tube spot welding investigated by 3D numerical simulations. Proceedings of the 7th International Seminar on Advances in Resistance Welding. Busan, Korea, p.147-158, 2012.